

Article

Antireflection Coating on PMMA Substrates by Atomic Layer Deposition

Pallabi Paul ^{1,†}, Kristin Pfeiffer ^{2,†} and Adriana Szeghalmi ^{1,2,*}

¹ Institute of Applied Physics, Abbe Center of Photonics, Friedrich Schiller University Jena, Albert Einstein Str. 15, 07745 Jena, Germany; pallabi.paul@uni-jena.de

² Fraunhofer Institute for Applied Optics and Precision Engineering IOF, Albert Einstein Str. 7, 07745 Jena, Germany; Kristin.Pfeiffer@iof.fraunhofer.de

* Correspondence: a.szeghalmi@uni-jena.de; Tel.: +49-3641-807-320

† These authors contributed equally to this work.

Received: 10 December 2019; Accepted: 7 January 2020; Published: 10 January 2020



Abstract: Antireflection coatings (ARC) are essential for various optical components including such made of plastics for high volume applications. However, precision coatings on plastics are rather challenging due to typically low adhesion of the coating to the substrate. In this work, optimization of the atomic layer deposition (ALD) processes towards conformal optical thin films of Al₂O₃, TiO₂ and SiO₂ on poly(methyl methacrylate) (PMMA) has been carried out and a five-layer ARC is demonstrated. While the uncoated PMMA substrates have a reflectance of nearly 8% in the visible (VIS) spectral range, this is reduced below 1.2% for the spectral range of 420–670 nm by applying a double-side ARC. The total average reflectance is 0.7%. The optimized ALD coatings show a good adhesion to the PMMA substrates even after the climate test. Microscopic analysis on the cross-hatch areas on PMMA after the climate test indicates very good environmental stability of the ALD coatings. These results enable a possible route by ALD to deposit uniform, crack free, adhesive and environmentally durable thin film layers on sensitive thermoplastics like PMMA.

Keywords: atomic layer deposition; antireflection coatings; PMMA; adhesion

1. Introduction

Thermoplastics like poly(methyl methacrylate) (PMMA), polycarbonate (PC) and polystyrene (PS) are widely used for producing various optical elements like freeform surfaces, aspheric lenses, Fresnel lenses and many other diffractive optical elements. In general, these substrates can be manufactured with significantly reduced cost compared to glass substrates by the well-established injection molding method. Because of being lightweight, the optical components made of plastics are an important substitute to glass optics. Among those, PMMA, which has a high transmission (~92%) in the visible spectral range (400–700 nm), excellent hardness, and high Abbe number is used extensively in precision optical manufacturing [1,2].

Thin film coatings are essential for precision optics to obtain various optical functions, e.g., antireflection coatings, dichroic mirrors, beam splitters, filters etc. However, precision coatings on plastics are rather challenging due to the crack formation and low adhesion of the dielectric coatings to the polymer surface [3]. Since the optimized process parameters for coatings on glass substrates cannot be directly transferred to the plastics, an explicit polymer-specific research is required to functionalize polymers.

Different deposition methods based on wet chemistry, physical vapor deposition (PVD) and chemical vapor deposition (CVD) techniques, such as sol-gel method [4], ion and plasma assisted PVD processes [5] and plasma enhanced chemical vapor deposition (PECVD) [6] have been applied

on PMMA and other plastic substrates with a motivation of enhancing their optical functionalities. Previous research suggests a special direct current (DC) glow discharge plasma pre-treatment [7,8], or a vacuum ultraviolet (VUV) protection layer by boat evaporation [9] prior to the plasma ion assisted depositions to improve the adhesion of thin films on PMMA. Several other approaches involving moth eye structures by full wafer and roll-to-roll nano-imprint lithography (NIL) [10], layer-by-layer assembly of hollow silica nanoparticles [11] and porous quarter wave antireflection coatings (ARC) with colloidal nanospheres [12] have also been demonstrated for ARC on plastics. Their environmental stability is rather limited, restricting the use of such coatings to the inner surfaces of the optical systems.

Nowadays, optical components are becoming increasingly complex. Examples of complex optics are highly curved, freeform, and aspheric lenses, domes, micro lens arrays, photonic crystal fibers, and many other non-planar 3D shapes. Achieving high-performance optical coatings on these complex substrates demands a development of thin film fabrication technology.

Atomic layer deposition (ALD) is a promising chemical coating technology for growing highly conformal thin films on strongly curved substrates. It is based on sequential and self-limiting surface reactions of the precursors with the available functional groups on the substrate surface. In contrast to the conventional PVD technologies, ALD can deposit uniform and conformal films even on complex 3D substrates or micro/nano-structured objects because of the self-saturating surface reactions and precise thickness control at nanometer range. In recent past, highly conformal antireflection coatings for strongly curved glass lenses, high-efficiency broadband antireflection (BBAR) coatings based on $\text{Al}_2\text{O}_3/\text{TiO}_2$ and $\text{SiO}_2/\text{HfO}_2$ multilayers, rugate notch filters, surface passivation layers for photovoltaic applications, antireflection coatings based on grass-like Al_2O_3 or nanoporous SiO_2 layers have been designed by ALD [13–20]. However, the materials and processes must be optimized to the particularities of plastics optics.

In this article, we present the development of ALD processes for adhesive and crack-free films on PMMA. Additionally, these films should be uniform in thickness, homogeneous and dense for application in optical coatings. Upon examining the optical properties (refractive index, optical losses) and mechanical stability of the films, a possible route for optical coatings (e.g., antireflection coating) shall be established via thermal ALD and plasma enhanced ALD (PEALD) processes. Finally, the 3D conformal growth of ALD films is exploited on PMMA domes, i.e., highly demanding complex shaped substrates.

2. Materials and Methods

2.1. Atomic Layer Deposition

The thin films were deposited using a commercial Oxford Instruments Plasma Technology (Bristol, UK) open load ALD reactor (OpAL™) equipped with an inductively coupled plasma (ICP) RF generator, operating at 13.56 MHz. Schematics of a similar experimental setup was presented by Faraz et al. [21]. Processes were developed to achieve a reproducible growth rate and optical properties along with a non-uniformity, NU < 5% on 200 mm area.

Al_2O_3 , SiO_2 and TiO_2 layers were grown on PMMA substrates using the commercially available metal-organic precursors (Strem Chemicals GmbH, Kehl, Germany) trimethylaluminium (TMA), tris(dimethylamino)silane (3DMAS) and titanium isopropoxide (TTIP). Thermal and PEALD processes are developed using H_2O and O_2 plasma, respectively. As PMMA has a glass transition temperature from 85 to 105 °C and melting point ~130 °C, the deposition temperature is kept at 60 °C (well below the polymer degradation temperature of PMMA) for all depositions.

2.2. Characterization Techniques

The refractive index and thickness of the films were determined on Si wafer substrates using spectroscopic ellipsometry (M2000, J.A. Woollam Co., Inc., Lincoln, NE, USA). The Cauchy model has been used to fit the psi and delta values in the spectral range from 400 to 1700 nm, whereby the

extinction coefficient, k is fixed to zero. The $NU = (d_{\max} - d_{\min})/2d_{\text{average}} \times 100\%$ is estimated from measurement at five positions on samples distributed over a 200 mm diameter area.

The reflectance (R) and transmittance (T) were recorded using a dual-beam ratio recording spectrophotometer Lambda 950 from Perkin Elmer™ (Waltham, MA, USA) with an in-house developed VN-device for absolute R -measurements. The absolute values of R and T are measured in the wavelength range of 400–800 nm within 0.2% of measurement accuracy. The optical losses (OL%) are defined as $= 100 - (T + R)$.

An Olympus K. K. USPM-RU-W NIR micro-spectrophotometer (Olympus Corporation, Tokyo, Japan) was used to measure the reflectance on different positions along the surface of the PMMA dome, where, the dome is placed on a tilt stage and tilted to angles up to 70° in four different directions. The incident light is focused with an objective (10 \times) on the surface of the substrate.

The adhesion properties of the optical coatings were evaluated with an adhesive tape (Tape 3M853) test according to the ISO 9211-4 02 method and the cross-hatch test according to the ISO 9211-4 03 method, respectively. The climate test was performed using a climate test chamber (BINDER GmbH, Tuttlingen, Germany) to examine the environmental stability of the antireflection coatings on PMMA. The environmental conditions were set at 16 h, 55 °C and 95% relative humidity. To examine the UV stability of the coatings, the spectral response of a double-sided coated PMMA was measured before and after UV exposure at 350 nm central wavelength for 24 h.

3. Results and Discussions

3.1. Development of ALD Processes on PMMA Substrate

PMMA is a loosely packed polymer and may trap TMA or water within the pores as discussed in [22–24]. Wilson et al. [23] reported that during the initial cycles (up to ~15 cycles), TMA and H₂O may diffuse into the pores and are difficult to fully purge from the reactor before the next reactant is pulsed. This can deteriorate the self-limiting characteristic of the ALD technique and hence the film growth and uniformity of the ALD films on PMMA. Chen et al. [25] showed that a hybrid vapor-phase infiltration (VPI) interphase is formed between the ALD Al₂O₃ film and PMMA due to the diffusion and the entrapment of the gas phase reactants within the polymer chains. Gradually, when a thin Al₂O₃ is formed on top of the PMMA, a linear growth of ALD film (after ~15 cycles) was observed.

Additionally, PMMA substrates are known to be sensitive to a plasma exposure. Schulz et al. [8] detected the complete loss of the ester –CH₃ groups at the polymer surface along with new signals of –CH₂ and –OH groups occurring upon a DC glow discharge plasma treatment of PMMA. The VUV emission of plasma significantly degrades the PMMA. Photons of energy ~8.5 eV (145 nm) can split off the methyl ester group, whereas the main polymer chain breaks at higher energy [26]. Kääriäinen et al. [27] observed that PMMA samples pre-coated with 33 nm Al₂O₃ or 55 nm TiO₂ layer deposited by thermal ALD processes show better adhesion of sputtered Ti coatings and less deviation in the attenuated total reflection-Fourier transform infrared (ATR-FTIR) absorption spectra than the untreated (bare) PMMA upon plasma exposure. Chen et al. [25] also explored the ability of thermal ALD Al₂O₃ films to enhance interfacial adhesion on PMMA by tuning the interfacial roughness. This motivated to deposit a ‘pre-coating’ of the Al₂O₃ layer in a thermal ALD process, since our preliminary coatings on PMMA by PEALD have led to poorly adhesive coatings.

The growth per cycle (GPC), refractive index (n) and film thickness (d) of the thermal ALD of Al₂O₃ coatings on Si wafer are presented in Table 1. The thermal Al₂O₃ process at a deposition temperature (T) = 100 °C has a GPC of 0.980 Å/cycle and a thickness non-uniformity of $NU = 1.07\%$ on a 200 mm diameter area. In comparison, the ALD process at 60 °C with increased purge times shows a higher GPC of 1.627 Å/cycle along with above 10% NU. The higher NU is probably due to CVD reactions of excess TMA and H₂O absorbed in the pores of the PMMA substrate. By applying larger purge times and an extra pump down step after the TMA and H₂O pulses, the non-uniformity was

substantially reduced to 5%. This is sufficient for meeting the AR target film thickness requirements, and these process parameters have been applied as the first layer in the AR stack.

Table 1. Atomic layer deposition (ALD) process parameters of thermal Al₂O₃ and characterizations.

T (°C)	ALD Cycle (s)			GPC (Å/Cycle)	NU (%)	n	d (nm)
	[Pulse]	[Pump]	[Purge]				
100	[0.02]	[6]	[0.03]	0.980	1.07	1.62	~50
60	[0.02]	[20]	[0.03]	1.627	10.5	1.55	~35
60	[0.02]	[20]	[60]	1.364	5.26	1.57	~40

The plasma enhanced ALD processes of SiO₂ and TiO₂ films were prepared on bare PMMA and 40 nm thermal Al₂O₃ pre-coated PMMA substrates for comparison. Choice of the plasma parameters plays the key role on the quality of the films. When a higher O₂ plasma gas flow is applied, the chamber pressure as well as the collision probability among the O⁺ ions and gas molecules increase; as a result, they bombard the substrate surface with less energy, decreasing the chance of degradation of the substrate [28]. Two different plasma parameters were chosen 300 W, 50 sccm (hereafter termed as ‘high’ plasma) and 100 W, 90 sccm (hereafter termed as ‘low’ plasma) (see Table 2). For the PEALD Al₂O₃ layer, when it was deposited on Si wafers and PMMA samples together in the chamber with ‘low’ plasma, it gave rise to higher GPC and NU. Whereas, when the deposition was done only on Si wafers, excluding the PMMA samples, keeping all the process parameters intact, NU can be improved from 7% to 1.1%. This indicates the disturbing influence of the PMMA substrate on the ALD processes. The process parameters of PEALD Al₂O₃, SiO₂ and TiO₂ are summarized in Table 2. A schematic diagram to explain the ALD cycle times (e.g., pulse, pump down, hold, and purge times) of thermal Al₂O₃, PEALD Al₂O₃, SiO₂ and TiO₂ processes mentioned in Tables 1 and 2 is represented in Figure 1. The cycle time of the thermal alumina layer is significantly longer than for the PEALD layers. Hence, this layer should be kept as thin as possible, to reduce the deposition time.

Table 2. Plasma enhanced ALD (PEALD) process parameters at 60 °C.

O ₂ Plasma Power, Flow Rate	ALD Cycle (s)		
	[Pulse]	[Purge]	[Pulse]
300 W, 50 sccm	[0.4 + 4 (hold)]	[10]	[3]
100 W, 90 sccm	[0.4 + 4 (hold)]	[10]	[3]

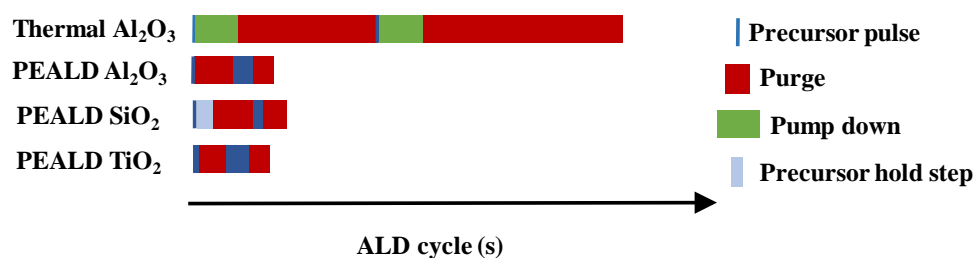


Figure 1. Schematic diagram of ALD cycle times for depositing thermal Al₂O₃, PEALD Al₂O₃, SiO₂ and TiO₂ films at 60 °C.

The GPC, NU, *n* and *d* of the PEALD processes are summarized in Table 3. PEALD processes have higher growth rate and hence will be preferred for the proposed AR coatings to produce the top layers which are not typically on the bare PMMA surface. Two different process conditions are applied for the SiO₂ and TiO₂ coatings. At a higher plasma power and a relatively low O₂ flow, the films show no substantial difference in terms of the film thickness, NU and refractive index.

Table 3. PEALD of Al₂O₃, SiO₂, TiO₂ coatings at 60 °C.

Films	O ₂ Plasma	GPC on Si Å/Cycle	NU (6 th) (%)	<i>n</i> at 632.8 nm	<i>d</i> (nm)	Crack Formation on Bare PMMA	Crack Formation on Pre-Coated PMMA	Adhesion on Bare PMMA	Adhesion on Pre-Coated PMMA
Al ₂ O ₃	low	1.56	1.11	1.60	~80	no	–	no	–
SiO ₂	high	1.29	0.92	~1.44	~40	yes	no	no	no
SiO ₂	low	1.31	1.31	~1.44	~40	no	no	no	yes
TiO ₂	high	0.45	4.48	~2.26	~55	yes	no	no	no
TiO ₂	low	0.45	4.80	~2.29	~55	no	no	no	yes

3.2. Optical Properties

The optical properties of the prepared films are investigated in order to apply them in the AR design on PMMA. Figure 2 gives a comparison of refractive indices of SiO₂, TiO₂ and Al₂O₃ films, which have been prepared at different temperatures and plasma conditions. Additionally, the refractive index of thermal TiO₂ deposited at 80 °C is plotted. Refractive indices of PEALD films prepared at 60 °C are in good agreement with the results from PEALD processes deposited at 100 °C temperature keeping other process conditions intact. For SiO₂, it is observed that the refractive index of the deposited films at 60 °C is slightly lower than at 100 °C by ~1%. The refractive index of SiO₂ films at 60 °C is still approximately 1.44 at 632.8 nm. The TiO₂ processes show a similar trend. A refractive index of ~2.25 at 632.8 nm is achieved in the PEALD process at 60 °C, which is significantly higher than that of TiO₂ deposited in thermal ALD process at 80 °C (*n* ~ 2.10 at 632.8 nm). Using water as an oxidizing agent leads to less dense films and consequently a lower refractive index. It is noticed that PEALD processes of TiO₂ enable the deposition of denser films even at lower temperature due to the high reactivity provided by the plasma radicals [29]. Since the difference of refractive indices between the low and high index materials should be as high as possible, the high refractive index material TiO₂ is preferably used for enhanced performance of antireflection coating on PMMA substrates. Additionally, thermal processes at 60 °C require much longer purge times to completely remove the H₂O, residual precursor and reaction by-products. This would lead to extremely long process times.

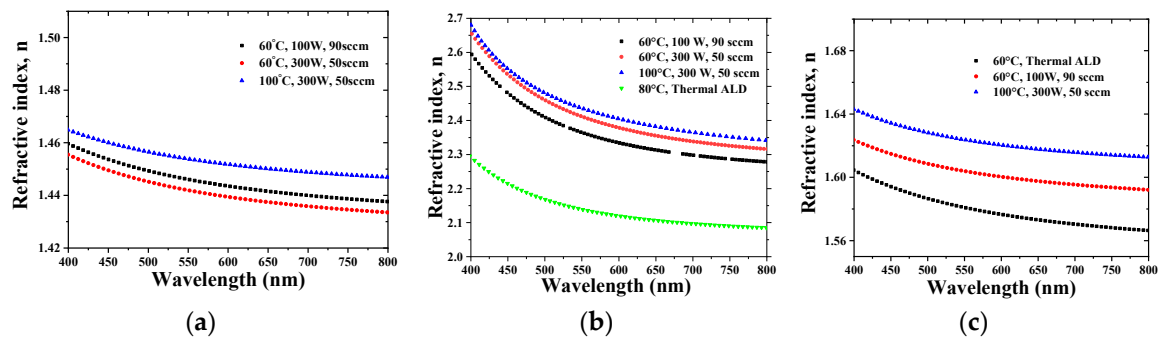


Figure 2. Refractive index (*n*) vs. wavelength for (a) SiO₂, (b) TiO₂ and (c) Al₂O₃ films at different temperature and plasma conditions.

The refractive index vs. wavelength of thermal and PEALD Al₂O₃ films have been plotted in Figure 2c for different process conditions. The refractive index of thermal Al₂O₃ film deposited at 60 °C is ~1.57 at 632.8 nm wavelength, whereas, the PEALD Al₂O₃ film at 60 °C with 100 W, 90 sccm of O₂ plasma flow gives rise to a refractive index of ~1.61 at 632.8 nm. The PEALD Al₂O₃ film deposited at 100 °C with 300W, 50 sccm O₂ plasma parameters possesses the highest refractive index of ~1.63 at 632.8 nm.

The optical losses (OL) of the individual films have been determined from the transmittance (*T*) and reflectance (*R*) data obtained by UV/VIS spectrophotometry measurements. The OL of SiO₂ thin films deposited at 60 °C are slightly increased compared to the layers grown at 100 °C indicating increasing impurity levels (N or C) in the layers with decreasing deposition temperature. However, the change of

OL is mainly relevant for the UV spectral range. The absorption edge shifts from approximately 200 to 230–240 nm wavelength for the films grown at 100 and 60 °C, respectively. The XPS and Auger electron spectroscopy analysis of SiO₂ thin films grown at 100 °C indicate very low impurity levels of around 0.1% for both N and C [30], whereas the depth profile analysis of nanoporous SiO₂ layers developed at 150 °C also shows low (1%) C impurities [19]. The surface contamination with C due to adsorbed hydrocarbons is significantly larger (approximately 3%) than the impurities in the film.

3.3. Mechanical Stability

Film adhesion tests (tape test and cross-hatch test) were performed to evaluate the adhesion of the films on the PMMA substrates. The visual and optical microscopic inspection indicates that 40 nm SiO₂ and 55 nm TiO₂ films deposited on bare PMMA substrates are peeled-off just after the tape test. In contrast, the SiO₂ and TiO₂ films deposited using the ‘low’ plasma conditions on pre-coated PMMA samples with 40 nm thermal Al₂O₃ show no significant delamination of the film after the cross-hatch test (see Table 3). The films deposited using the ‘high’ plasma conditions show cracks and poor adhesion on both bare and Al₂O₃ pre-coated PMMA samples.

The optimization of the plasma conditions has been essential to improve the adhesion of coatings on PMMA. The increase of O₂ plasma flow rate from 50 to 90 sccm and the reduction of O₂ plasma power of the ICP generator from 300 to 100 W decrease the intensity of the O⁺ bombardment on the PMMA substrates. The self-bias potential decreases from about 5 to 2.5 V, while the intensity of UV emission does not change significantly [28]. The vacuum UV radiation of the ICP plasma is fully or partially absorbed by the thermal Al₂O₃ layer pre-coating. The thermal Al₂O₃ layer may also protect the PMMA substrate from the ion bombardment suggesting that minute changes in the film properties are relevant. Additionally, the strong interfacial bonding between the organic PMMA surface and the thermal ALD inorganic Al₂O₃ layer directly on PMMA seems to be the main reason for achieving adhesive ALD films on PMMA, which has been one of the main challenges in realizing optical coatings on PMMA.

3.4. Antireflection Coatings

3.4.1. Design

A five-layer antireflection design is simulated for PMMA substrates using the OptiLayer software (version 12.83g, OptiLayer GmbH, Garching, Germany). The desired wavelength range is from 420 to 670 nm. A design consisting of Al₂O₃ (t)/TiO₂ (p)/Al₂O₃ (p)/TiO₂ (p)/SiO₂ (p) is applied, where (t) and (p) stand for thermal and plasma-enhanced processes, respectively. The first thermal Al₂O₃ layer ensures good adhesion of the coatings and the safest process on plasma sensitive PMMA substrates. Another plasma enhanced Al₂O₃ layer has been incorporated between two thin TiO₂ layers to avoid crystallization of thick TiO₂ films [28]. In addition, it serves the purpose of reducing the total thickness of TiO₂ layer, which has a low GPC and to improve the optical performance of the ARC. The PEALD alumina is a preferred intermediate refractive index layer instead of the low refractive index PEALD silica because its growth rate is higher and provides a more robust process. The last layer is made of SiO₂, a low refractive index material to significantly enhance the antireflection performance. The O₂ plasma parameters were chosen at 100 W plasma power and 90 sccm O₂ gas flow for the antireflection coating.

3.4.2. ARC on PMMA Plates

Figure 3a shows the reflection spectra of the double-sided AR-coated and bare PMMA substrates, where, the red-dashed curve indicates the AR design simulated by OptiLayer and the solid black curve shows the resultant spectrum of the AR-D1 coating. In Figure 3a, a difference between the spectra of the AR design and the experimental AR-D1 coating can be noticed. This is due to deviations of the growth rates. The GPC values were determined on Si substrates. Furthermore, the growth rate of the TiO₂ film has been determined from a thicker layer than the one used in the ARC. The thicknesses of

layers in the AR system are probably deviating from the expected values due to a different growth on a Si substrate than on the bare PMMA or ALD sub-layers and due to a nucleation delay of TiO₂.

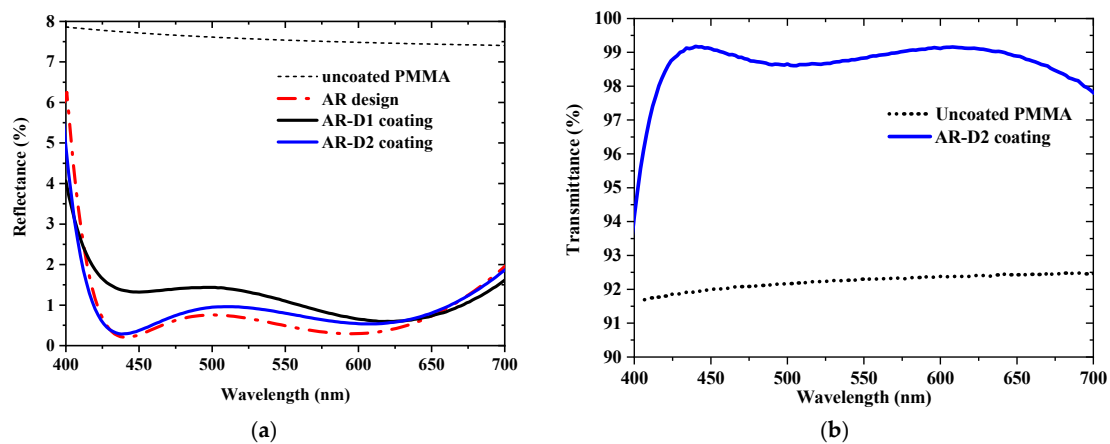


Figure 3. (a) Reflection spectra of AR design (red-dashed curve) and double-sided AR coated PMMA samples, i.e., AR-D1 (black solid curve) and AR-D2 (blue solid curve). Reflectance of uncoated PMMA substrate (dotted line) is given for comparison. (b) Transmittance spectra of bare and double-sided AR coated PMMA sample.

In order to estimate the actual thickness and GPC of each layer during the AR-D1 deposition, a recalculation was performed using the experimental reflection spectrum of AR-D1 with the OptiRE software (version 12.83g, OptiLayer GmbH, Garching, Germany). The first thermal Al₂O₃ layer on PMMA has little influence on the spectral property of the five layer stack, as its refractive index is similar to that of PMMA. Consequently, the thickness of this layer has been kept fixed during recalculation. Further, the refractive indices of the individual layers were kept constant. The best fit to the experimental AR-D1 curve indicates a thinner TiO₂ layer than desired, whereas SiO₂ and PEALD Al₂O₃ grew thicker than the design target (see Table 4). Thus, TiO₂ has a lower growth rate, and PEALD Al₂O₃ and SiO₂ have a higher growth per cycle on ALD sub-layers than on the native SiO₂ layer of the Si wafer. Using the re-calculated GPC values, the necessary cycles for the AR coating were newly calculated and the AR-D2 coating was deposited accordingly. The optical performance of the second AR coating (AR-D2) (see blue curve in Figure 3a) is in a very good agreement with the design. This indicates that the ALD processes are well understood and controlled since the deposition is carried out without in situ monitoring. A reflectance (R) below 1.2% can be achieved for the spectral range of 420–670 nm with an average reflectance (R_{av}) minimized to ~0.7%, whereas the bare substrate has a R_{av} of nearly 8%. The average transmittance can be increased from 92% to an average of ~99% (Figure 3b) and average optical losses are ~0.3% in the same spectral range.

Table 4. Target layer thickness and necessary ALD cycles for AR coating on PMMA.

Material	Design (nm)	ALD Cycles (AR-D1)	Recalculated Thickness (nm)	Recalculated GPC (Å/Cycle)	Recalculated ALD Cycles (AR-D2)
Al ₂ O ₃ (t)	94.5	693	(fixed)	1.364	693
TiO ₂ (p)	17.3	381	14.5	0.380	455
Al ₂ O ₃ (p)	45.1	290	48.0	1.655	272
TiO ₂ (p)	23.7	522	19.8	0.380	627
SiO ₂ (p)	105.1	815	110.0	1.350	779

After the successful preliminary investigations of ARC via ALD on PMMA plates, this design is extended to 3D PMMA substrates, e.g., PMMA domes to investigate the 3D conformality of the ALD processes on more complex substrates. Dome substrates have been selected in order to assess the uniformity of the ALD coatings on the inner and outer sides of large 3D objects. The precursor

and plasma species must be well distributed within the reactor even though these are introduced and produced in the top region above the substrates. The rear-side of the substrates should be coated in the same quality despite the fact that it is not directly facing the plasma.

3.4.3. PMMA Domes

The same five-layer AR-D2 coating has been deposited on PMMA domes with a diameter of 50 mm and a height of 25 mm. The reflectance (R) of the dome's surface is measured by a micro-spectrophotometer in four different directions up to 70° angular positions along the outer surface and at the center of the inner surface. In Figure 4a, the solid black and green curves show the measured reflectance spectra of the center positions of inner and outer surfaces, respectively, which are quite consistent with each other. Likewise, the measured spectra at center and 70° inclined positions in four directions (north, east, south, and west) along with the center of the inner surface are also nearly identical indicating a promising 3D conformality of these ALD processes.

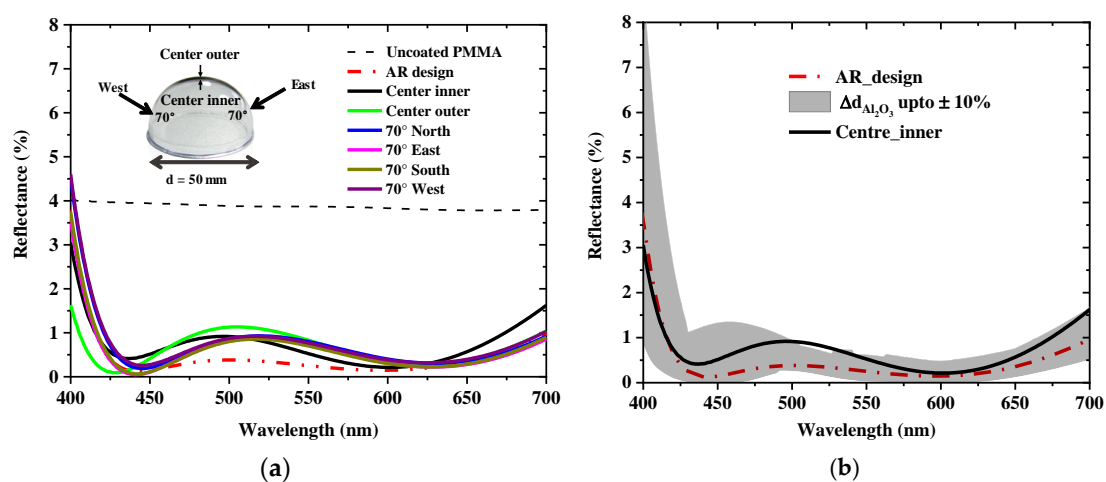


Figure 4. (a) Measured reflectance at the center positions of the outer and inner surfaces of the PMMA dome and reflectance at 70° tilted position of the dome in four directions on the outer surface, (b) Reflectance at the center position of the inner surface of PMMA dome along with the AR design and 10% tolerance of Al_2O_3 film thicknesses.

However, the reflection spectra of the dome show substantial deviation from the targeted design (see Figure 4a) around 500 nm wavelength despite of using the same number of cycles as in AR-D2 (see Table 3). The coating of the domes was performed approximately four months after the previous AR-D2 process on PMMA plates. A significantly higher GPC of Al_2O_3 is predicted in this process, which became more prominent in some other contemporary processes in the same ALD tool. In Figure 4b, an error corridor for the residual reflectance spectra was calculated assuming a 10% thickness variation in case of Al_2O_3 deposition (grey shaded area) and the obtained spectrum lies within the assumed range.

The higher GPC of Al_2O_3 may have its origin in a parasitic CVD type reaction of TMA with water during TMA pulse, leading to a higher growth rate. This suggests a leak in the tool. Indeed, a thorough check of the tool determined leakage of the equipment at several positions. The precursor, purge and pump lines of the ALD tool were 'leak' tested. A substantially higher leak rate was observed for the TMA line reaching ~ 7 instead of ~ 2 mTorr/min. The higher leak rate suggests an uncontrolled reaction between the TMA and water. This assumption is supported by an additional test, so-called 'water test', in which only TMA is pulsed for 30 ms into the chamber, repeated by 500 cycles. In case of a leak, H_2O from the environment can enter the reactor. This test led to a deposition of thin Al_2O_3 film of ~ 12 nm average thickness. Since, ideally, 'water test' should not produce any deposition because of no oxidizing precursor (i.e., no formation of Al_2O_3), this result confirms the malfunctioning of the

equipment. After replacement of the valve and cleaning the tool, the deposited layer thickness turned out to be ~1–2 nm during the ‘water test’. These results are discussed here in order to highlight the sensitivity of these AR coatings to changes in the conditions of the reactor.

After improving the conditions of the equipment, the AR coating has been repeated. Reflection spectra of this ARC on different positions of PMMA dome are depicted in Figure 5. Optical properties on the center positions of inner and outer surfaces along with 70° inclined positions on the outer surface in four directions (north, east, south, and west) are in excellent agreement with the antireflection design. The reflectance spectra on curved dome surfaces show promising uniformity and 3D conformality within 1–5% NU across the deposition chamber (Table 3).

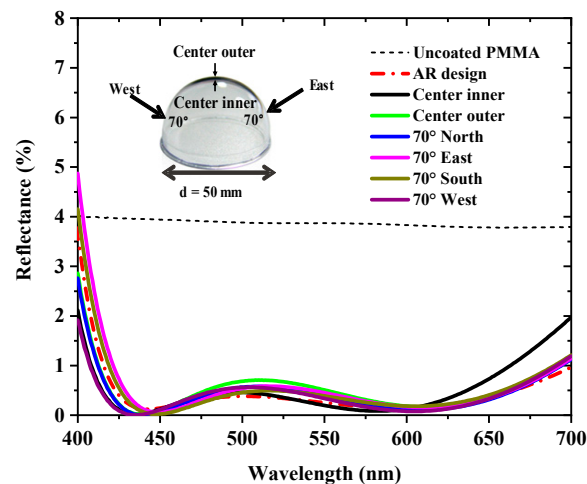


Figure 5. Measured reflectance spectra at the center positions of the outer and inner surfaces of the PMMA dome and at 70° inclined positions in four directions along the outer surface exhibit excellent 3D conformality of ALD coatings.

3.4.4. Environmental Durability and Mechanical Stability

PMMA is highly sensitive to different climatic conditions, e.g., temperature, humidity, UV exposure, etc. Therefore, it is necessary to examine the environmental and UV stability of these AR coatings on PMMA. A climate test for 16 h at 55 °C with 95% of relative humidity according to ISO 9022-2 was performed on the double-sided coated PMMA of AR-D2. There is no significant change in the reflection spectra after the climate test (see Figure 6), which indicates a good environmental stability of ARC on PMMA prepared by ALD.

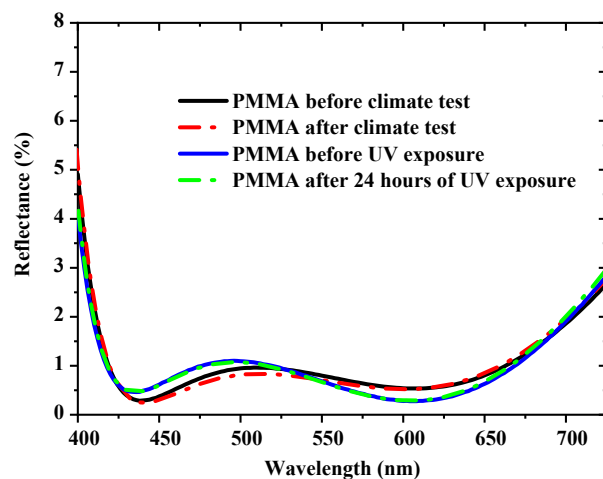


Figure 6. Comparison of the reflectance spectra of double-sided AR coated PMMA of AR-D2 before and after climate test and before and after 24 h of UV exposure.

ALD coatings are highly reproducible. Thirty (30) AR samples on PMMA were prepared in a span of ~6 months and the results are very similar except some minor changes due to lateral thickness non-uniformity across different positions on the deposition chamber. Another double-sided AR-coated PMMA (deposited approximately half-year after the AR-D2 on PMMA plates, Figure 3) is exposed to UV radiation for 24 h. From the visual appearance, the AR coated PMMA sample had no degradation or change in color after UV radiation. The spectral response before and after the UV exposure (see Figure 6) confirm the UV stability of ALD coatings on PMMA. The results of UV stability may rely on the fact of partial or complete absorption of UV radiation by the dielectric coatings, whereas bare PMMA starts degrading under UV radiation [26].

Cross-hatch tests were performed to check the adhesion of the AR coatings on PMMA, since both passed the tape test. Figure 7 shows microscopic images of the samples after the cross-hatch test. No delamination of the films (both sides) have been observed either on the AR-D1 double-sided coating or on the AR-D2 sample after climate test.

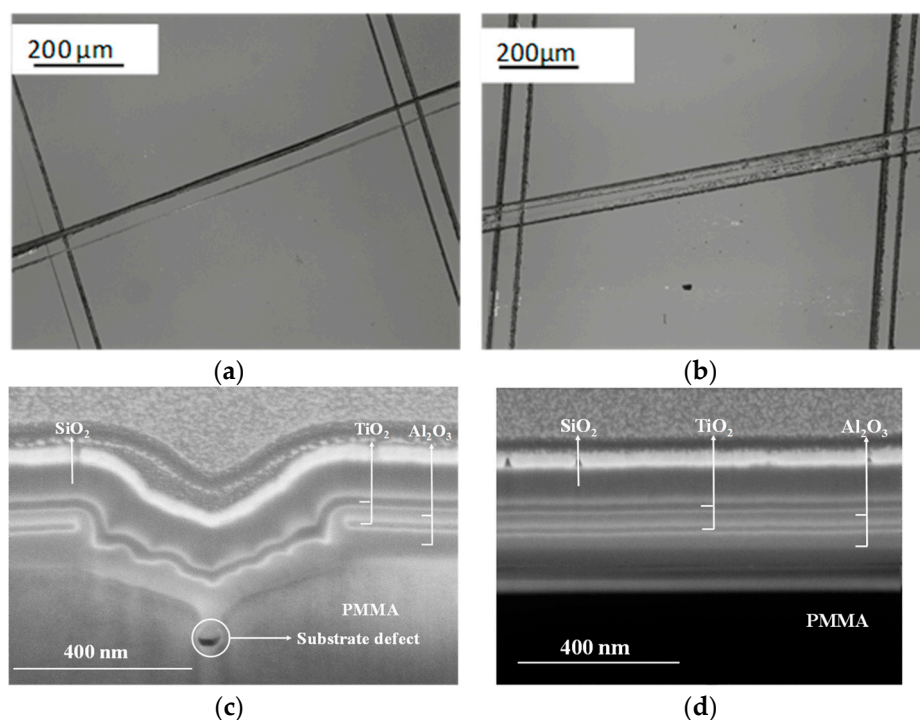


Figure 7. (a) Optical microscopic images after cross-hatch tests of AR-D1 double-sided coated PMMA, and (b) double-sided AR coating AR-D2 sample after climate test demonstrate their environmental stability, (c) focused ion beam scanning electron microscopy (FIB-SEM) cross-sectional image of single-sided five-layer AR coating on PMMA (focused on a crack), (d) FIB-SEM cross-sectional image of single-sided five-layer AR coating on PMMA (focused on a crack-free region).

Damage of the PMMA plates has been observed in some cases. On some samples, two or three crack lines are observed formed near the injection molding point. After the deposition of AR multilayer system, FIB-SEM (Helios NanoLab G3 UC, Thermo Fischer Scientific, Oregon, USA) images have been taken in order to observe the cross-sectional view of such defects. Figure 7c focuses on a crack of the five-layer AR-coated PMMA substrate indicating the substrate has some minute manufacturing defect (not visible without the coating) in that region. The thermal Al_2O_3 layer was successfully deposited on that region. As soon as the next PEALD TiO_2 layer has been deposited, the defect is enhanced and leads to a breakage of TiO_2 film around that region (the bottom TiO_2 layer is interrupted). The next PEALD Al_2O_3 layer compensates the separation of the previous layer, although it shows buckling at some points. Subsequently, the next PEALD TiO_2 and SiO_2 layers were deposited continuously on

the top. Despite the generation of stress due to the TiO₂ layer, the first thermal Al₂O₃ layer possesses a strong bonding with the PMMA substrate, which is the key reason for obtaining adhesive films on PMMA.

Figure 7d focuses on a crack-free region, where the ALD films are observed to be deposited uniformly. The FIB-SEM images denote that the probability of formation of cracks on sensitive PMMA substrates are higher on the region where the substrate is inherently having some manufacturing defect, i.e., so called 'weak' point or the region which inherently possesses more stress, for example, the injection molding point of the PMMA substrates.

4. Conclusions

Atomic layer deposition enables to develop adhesive, crack-free and conformal AR coatings on PMMA substrates. This requires the optimization of the process parameters and the characterization of single layer Al₂O₃, TiO₂, and SiO₂ ALD thin films on PMMA from the perspective of optical coatings. These films should possess certain qualities, such as thickness uniformity, homogeneity and most importantly be adhesive and crack-free on the highly sensitive optical thermoplastic PMMA. The growth rate of the thermal Al₂O₃ is ~0.03 nm/min, whereas PEALD Al₂O₃, TiO₂ and SiO₂ layers have a substantially higher growth rate of ~0.46, 0.14 and 0.33 nm/min, respectively, using the OpAL™ tool. Difficulties in coating PMMA substrates have been encountered due to the porous nature of this material. The TMA or H₂O precursor molecules are trapped in the pores of PMMA, which leads to parasitic CVD reactions. Longer purge times along with extra pump down steps during the deposition of thermal Al₂O₃ adhesion layer were employed to avoid the presence of excess water and reactant in the chamber. Additionally, improved plasma parameters for the top PEALD layers along with the thermal Al₂O₃ pre-coating have successfully enabled to deposit a crack-free, adhesive and environmentally durable (16 h, 55 °C, 95% rh) antireflection coating on PMMA substrates. With the proposed five-layer AR design and corresponding double-sided AR-coating, the reflectance has been reduced below 1.2% for the spectral range of 420–670 nm with an average reflectance minimized to 0.7%, whereas the average reflectance of the bare substrate is ~8%. The average transmission has been increased from 92% to ~99% between 420–670 nm wavelength. The optical losses are ~0.3% for the desired spectral range indicating no significant optical loss due to the thin film layer-stack. For these plasma-enhanced double-sided coatings, the backside is also evenly coated despite not facing the plasma unit directly. All these aforementioned process conditions lead to a good agreement between the designed and measured reflectance even on 3D curved PMMA domes. These results strongly motivate further research and development to establish AR coatings by ALD on 3D substrates, both on glass and plastics. The ALD technique is capable of depositing double-sided coating in a single process, which makes the process easier when the rear side coating is also desired, and it partly compensates for the long deposition time of ALD. The spectral properties at different positions along the surface of the dome show excellent 3D conformality without the need of in-situ thickness monitoring or complex substrate rotation. Hence, a great flexibility in the choice of substrate geometries is given by PEALD for high performance antireflection coatings.

Author Contributions: Conceptualization, A.S.; methodology, A.S. and K.P.; experiments, P.P. and K.P.; data analysis and interpretation, P.P., K.P. and A.S.; writing—original draft preparation, P.P.; writing—review and editing, all authors. All authors have read and agreed to the published version of the manuscript.

Funding: Funding of the Emmy Noether grant SZ253/1-1 of the Deutsche Forschungsgemeinschaft (DFG, German Research Foundation), and of the projects fo+ (grant No. 03WKCX1B) within the framework "Unternehmen Region—Innovative Regional Growth Cores" of the BMBF, KOSLAN (grant No. ZF4309604SY8) of the BMWi AiF Projekt GmbH, and Attract 601020 of the FhG is gratefully acknowledged.

Acknowledgments: We thank Ulrike Schulz for discussions and comments to our manuscript, Nancy Gratzke for assistance with stability testing, Stefan Fasold for the FIB-SEM investigations and David Kästner for technical assistance with the PEALD equipment.

Conflicts of Interest: The authors declare no conflicts of interest.

References

1. Schulz, U. Review of modern techniques to generate antireflective properties on thermoplastic polymers. *Appl. Opt.* **2006**, *45*, 1608–1618. [[CrossRef](#)] [[PubMed](#)]
2. Schulz, U.; Schallenberg, U.B.; Kaiser, N. Antireflection coating design for plastic optics. *Appl. Opt.* **2002**, *41*, 3107–3110. [[CrossRef](#)] [[PubMed](#)]
3. Schaffer, R.W. Problems and solutions for coating plastic optics. In *Replication and Molding of Optical Components*; Riedl, M.J., Ed.; SPIE: Bellingham, WA, USA, 1988; p. 140.
4. Chen, D. Anti-reflection (AR) coatings made by sol-gel processes: A review. *Sol. Energy Mater. Sol. Cells* **2001**, *68*, 313–336. [[CrossRef](#)]
5. Pulker, H.K. Optical coatings deposited by ion and plasma PVD processes. *Surf. Coat. Technol.* **1999**, *112*, 250–256. [[CrossRef](#)]
6. Martinu, L.; Poitras, D. Plasma deposition of optical films and coatings: A review. *J. Vac. Sci. Technol. A* **2000**, *18*, 2619–2645. [[CrossRef](#)]
7. Schulz, U.; Jaenchen, H.; Kaiser, N. Plasma pretreatment and coating of PMMA Fresnel lenses. In *Advances in Optical Interference Coatings*; Amra, C., Macleod, H.A., Eds.; SPIE: Bellingham, WA, USA, 1999; pp. 511–516.
8. Schulz, U.; Munzert, P.; Kaiser, N. Surface modification of PMMA by DC glow discharge and microwave plasma treatment for the improvement of coating adhesion. *Surf. Coat. Technol.* **2001**, *142–144*, 507–511. [[CrossRef](#)]
9. Munzert, P.; Schulz, U.; Kaiser, N. Method for the vacuum deposition of optical coatings on polymethyl methacrylate. *Plasma Process. Polym.* **2007**, *4*, S1036–S1040. [[CrossRef](#)]
10. Burghoorn, M.; Roosen-Melsen, D.; Riet, J.; Sabik, S.; Vroon, Z.; Yakimets, I.; Buskens, P. Single layer broadband anti-reflective coatings for plastic substrates produced by full wafer and roll-to-roll step-and-flash nano-imprint lithography. *Materials* **2013**, *6*, 3710–3726. [[CrossRef](#)]
11. Du, Y.; Luna, L.E.; Tan, W.S.; Rubner, M.F.; Cohen, R.E. Hollow silica nanoparticles in UV-visible antireflection coatings for poly(methyl methacrylate) substrates. *ACS Nano* **2010**, *4*, 4308–4316. [[CrossRef](#)]
12. Buskens, P.; Burghoorn, M.; Mourad, M.C.D.; Vroon, Z. Antireflective coatings for glass and transparent polymers. *Langmuir* **2016**, *32*, 6781–6793. [[CrossRef](#)]
13. Pfeiffer, K.; Schulz, U.; Tünnermann, A.; Szeghalmi, A. Antireflection coatings for strongly curved glass lenses by atomic layer deposition. *Coatings* **2017**, *7*, 118. [[CrossRef](#)]
14. Szeghalmi, A.; Helgert, M.; Brunner, R.; Heyroth, F.; Gösele, U.; Knez, M. Atomic layer deposition of Al₂O₃ and TiO₂ multilayers for applications as bandpass filters and antireflection coatings. *Appl. Opt.* **2009**, *48*, 1727–1732. [[CrossRef](#)] [[PubMed](#)]
15. Li, Y.; Shen, W.; Hao, X.; Lang, T.; Jin, S.; Liu, X. Rugate notch filter fabricated by atomic layer deposition. *Appl. Opt.* **2014**, *53*, A270–A275. [[CrossRef](#)] [[PubMed](#)]
16. Richter, A.; Benick, J.; Hermle, M. Boron emitter passivation with Al₂O₃ and Al₂O₃/SiN_x stacks using ALD Al₂O₃. *IEEE J. Photovolt.* **2013**, *3*, 236–245. [[CrossRef](#)]
17. Yu, I.-S.; Wang, Y.-W.; Cheng, H.-E.; Yang, Z.-P.; Lin, C.-T. Surface passivation and antireflection behavior of ALD on n-type silicon for solar cells. *Int. J. Photoenergy* **2013**, *2013*, 1–7. [[CrossRef](#)]
18. Kauppinen, C.; Isakov, K.; Sopanen, M. Grass-like alumina with low refractive index for scalable, broadband, omnidirectional antireflection coatings on glass using atomic layer deposition. *ACS Appl. Mater. Interfaces* **2017**, *9*, 15038–15043. [[CrossRef](#)]
19. Ghazaryan, L.; Sekman, Y.; Schröder, S.; Mühlig, C.; Stevanovic, I.; Botha, R.; Aghaee, M.; Creatore, M.; Tünnermann, A.; Szeghalmi, A. On the properties of nanoporous SiO₂ films for single layer antireflection coating. *Adv. Eng. Mater.* **2019**, *21*, 1801229. [[CrossRef](#)]
20. Pfeiffer, K.; Ghazaryan, L.; Schulz, U.; Szeghalmi, A. Wide-angle broadband antireflection coatings prepared by atomic layer deposition. *ACS Appl. Mater. Interfaces* **2019**, *11*, 21887–21894. [[CrossRef](#)]
21. Faraz, T.; Knoops, H.C.M.; Verheijen, M.A.; van Helvoirt, C.A.A.; Karwal, S.; Sharma, A.; Beladiya, V.; Szeghalmi, A.; Hausmann, D.M.; Henri, J.; et al. Tuning material properties of oxides and nitrides by substrate biasing during plasma-enhanced atomic layer deposition on planar and 3D substrate topographies. *ACS Appl. Mater. Interfaces* **2018**, *10*, 13158–13180. [[CrossRef](#)]
22. Steven, M.; George, J.; Ferguson, D.; Alan, W.; Weimar, C.; Wilson, A. Method of deposition an inorganic film on an organic polymer. U.S. Patent 9,36,750,B2, 28 June 2016.

23. Wilson, C.A.; Grubbs, R.K.; George, S.M. Nucleation and growth during Al₂O₃ atomic layer deposition on polymers. *Chem. Mater.* **2005**, *17*, 5625–5634. [[CrossRef](#)]
24. George, S.M. Atomic layer deposition: An overview. *Chem. Rev.* **2010**, *110*, 111–131. [[CrossRef](#)] [[PubMed](#)]
25. Chen, Y.; Ganga, N.J.; LePage, W.S.; Kazyak, E.; Gayle, A.J.; Wang, J.; Rodríguez, R.E.; Thouless, M.D.; Dasgupta, N.P. Enhanced interfacial toughness of thermoplastic-epoxy interfaces using ALD surface treatments. *ACS Appl. Mater. Interfaces* **2019**. [[CrossRef](#)]
26. Schulz, U. Coating on plastics. In *Handbook of Plastic Optics*, 2nd ed.; Bäumer, S., Ed.; Wiley-VCH: Weinheim, Germany, 2010; pp. 161–195. ISBN 9783527635443.
27. Kääriäinen, T.O.; Cameron, D.C.; Tanttari, M. Adhesion of Ti and TiC coatings on PMMA subject to plasma treatment: Effect of intermediate layers of Al₂O₃ and TiO₂ deposited by atomic layer deposition. *Plasma Process. Polym.* **2009**, *6*, 631–641. [[CrossRef](#)]
28. Ratzsch, S.; Kley, E.B.; Tünnermann, A.; Szeghalmi, A. Influence of the oxygen plasma parameters on the atomic layer deposition of titanium dioxide. *Nanotechnology* **2015**, *26*, 24003. [[CrossRef](#)] [[PubMed](#)]
29. Profijt, H.B.; Potts, S.E.; van de Sanden, M.C.M.; Kessels, W.M.M. Plasma-assisted atomic layer deposition: Basics, opportunities, and challenges. *J. Vac. Sci. Technol. A* **2011**, *29*, 50801. [[CrossRef](#)]
30. Beladiya, V.; Becker, M.; Faraz, T.; Kessels, W.; Schenk, P.; Otto, F.; Fritz, T.; Gruenewald, M.; Helbing, C.; Jandt, K.D.; et al. Effect of electric field during deposition of silicon dioxide thin films by plasma enhanced atomic layer deposition: Experimental and computational study. *Nanoscale* **2020**. [[CrossRef](#)]



© 2020 by the authors. Licensee MDPI, Basel, Switzerland. This article is an open access article distributed under the terms and conditions of the Creative Commons Attribution (CC BY) license (<http://creativecommons.org/licenses/by/4.0/>).